MODELING INSOLATION-DRIVEN AEOLIAN ACTIVITY IN MERIDIANI PLANUM IN THE LAST 400 KA. Fenton[1], L. K. and Michaels[2], T.M. [1]Carl Sagan Center at the SETI Institute, 189 Bernardo Ave., Ste. 100, Mountain View, CA 94043, USA, lfenton@carlsagancenter.org, [2]Southwest Research Institute, 1050 Walnut St., Ste. 300, Boulder, CO, USA, tmichael@boulder.swri.edu.

Introduction: Over the course of Mars' history, the wind has played a major role in both sculpting the landscape and recording the planet's climate variations. Bedforms (e.g. dunes, ripples) in some locations appear to be actively migrating today [e.g., 1-3]; others are considered inactive [e.g., 4-5]. Although it is agreed that many stabilized aeolian features were once active under different climatic conditions, it is not known how old most aeolian bedforms are or what conditions are required to remobilize them. The only well-constrained ancient period of bedform migration has been identified for coarse-grained ripples in Meridiani Planum, which are thought to have last been mobile in the period ~50-200 ka [6]. It was proposed in [6] that changes in Mars' orbital state prior to ~50 ka may have influenced wind speeds enough to account for this shift in aeolian activity. We discuss initial results from testing this hypothesis with a global climate model (GCM). Another abstract from this meeting describes initial results from mesoscale model simulations addressing the same hypothesis [7].

Wind Regime in Meridiani Planum:

Present-day: Coarse-grained ripples cover much of the terrain in Meridiani Planum. In the current epoch the ripples appear to be inactive [6,8,9]. However, there is abundant evidence for active saltation, including the erasure of rover tracks [10], observed changes in wind streaks [11], and nearby dune migration and erosion [12]. Although the MER Opportunity is not equipped with atmospheric sensors, estimates of wind direction, strength, and relation to weather patterns may be inferred from other data sets. Episodic winds from the northwest seem to be qualitatively correlated with planetary-scale dust events, whereas weaker but more continuous winds from the southeast to south-southeast seem to otherwise dominate sand transport (they are active at least during local fall, winter, and early spring). Inside Endeavour crater, southeast of Opportunity's traverse, easterly winds also transport sand; however it is unclear whether these winds transport sand elsewhere in Meridiani Planum. Winds with friction speeds greater than ~3-3.5 m/s are thought to be capable of reactivating the coarse-grained ripples [13,14], so it is likely that the winds described above are not this strong.

~50-200 ka: The coarse-grained ripples are aligned nearly north-to-south (N4ºE), formed by wind from the east (see Fig. 1) [8, 13]. Ripple crests show the initiation of a realignment to northeast-to-southwest (N38ºE) [13], but it is unclear whether these winds blew from the NW or the SE (for example, they could correspond to the present-day episodic winds from the NW or the more continuous winds from the SE to SSE).

It is important to note that the techniques used to infer past- and present-day wind regimes in Meridiani Planum are different and are likely to provide incomplete information regarding the wind regime. For example, both dark and bright wind streaks vary on seasonal timescales or less, whereas the coarse-grained ripples likely required many years (perhaps decades to centuries) to respond to changes in wind patterns. This "apples-to-oranges" comparison may influence analysis of GCM simulations.

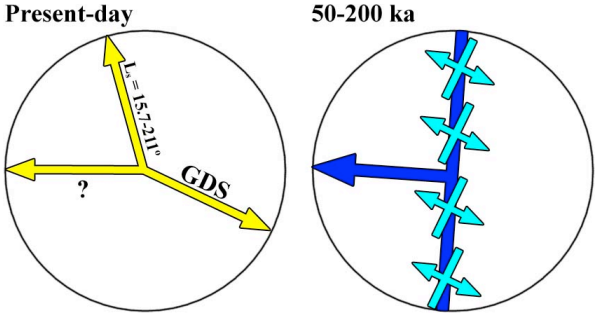

Figure 1. Inferred wind regimes in Meridiani Planum.

Recent Insolation States in Meridiani Planum: A model of the time evolution of Mars' orbital state (described by its orbital eccentricity, season of perihelion, and axial obliquity) determines how the planet's "insolation state" has varied in the past [15]. In the last 400 ka, the local season of maximum insolation has varied throughout the year (see Fig. 2). In that time the axial obliquity has ranged from 20.11º to 30.56º, but in the last 200 ka it has only varied between 22.11º and 26.67º (within -12% to 6% of the present-day value of 25.19º). In contrast, the eccentricity has varied between 0.0602 and 0.1177 (within -35% to 26% of the present-day value of 0.0933). Perhaps most strikingly, precession has caused the L_s of perihelion to pass through each season nearly eight times. Thus, three factors appear to most strongly control insolation in the recent martian past: season, L_s of perihelion, and eccentricity.

The insolation state has a strong influence on both the magnitude and the season of peak insolation at the

latitude of Meridiani Planum (bottom panel of Fig. 2). At present, Meridiani Planum receives maximum insolation during local (southern) summer and minimum insolation during winter. Periods during which the maximum annual insolation occurs during summer solstice, winter solstice, and the equinoxes are marked with vertical lines. These periods of extreme insolation may represent "end-members", bracketing the likely atmospheric responses to change in orbital state. As a result, these insolation states are the first targets of our study.

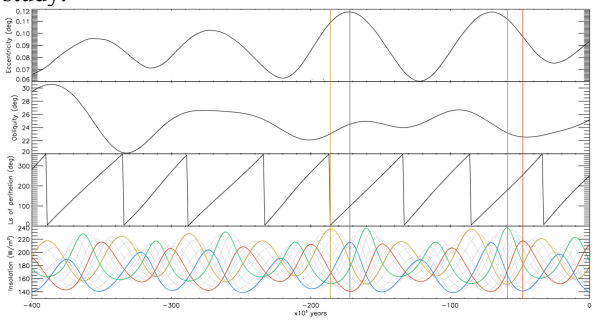

Figure 2. Top three panels show Mars' eccentricity, obliquity, and L_s of perihelion over the last 400 ka. The bottom shows daily mean insolation at the latitude of Meridiani as a function of season: L_s = 0º (green), L_s = 90º (blue), L_s = 180º (orange), L_s = 270º (red). Note that the peak insolation varies with season and does *not* always correspond to local summer.

GCM and simulations: A global climate model predicts a time-dependent, plausible state of the atmosphere, surface, and subsurface by integrating forward in time the physical equations of motion, thermodynamics, radiative transfer, and other processes, constrained by observation-based knowledge and datasets. The relatively few previous studies that have briefly discussed or modeled the impact of one or more insolation parameters on near-surface winds in Mars' near past have employed GCMs. In general, those prior studies suggest that wind stresses vary with at least axial obliquity, potentially enhancing or inhibiting aeolian processes [16-18]. Two of these studies found that large-scale global wind patterns are invariant to changes in obliquity [16,17]. However, the modeled winds were presented as seasonal averages [16] or diurnal averages [17], either of which could easily mask strong but short-lived flows that could be responsible for intense aeolian activity.

To predict the wind regime in Meridiani Planum, we used the NASA Ames GCM (version 2.1) [19-21]. This hydrostatic model utilizes a 5ºx6º horizontal grid with 24 vertical levels (more numerous within the boundary layer than aloft). This model explicitly predicts the CO_2 and H_2O cycles (including water-ice cloud microphysics, although in the simulations discussed here this was not included). The GCM predicts the atmospheric dust loading as a function of season, latitude, longitude, and altitude (for contemporary Mars this is based on Mars Global Surveyor Thermal Emission Spectrometer dust opacity data from Mars Year 26). In each simulation, output was saved sixteen times per day for an entire martian year (after running five martian years to allow the model to spin up).

We ran the GCM under four different orbital configurations from the past 400 ka: those producing maximum insolation during local summer solstice (i.e., present-day), winter solstice, autumnal equinox, and vernal equinox (see Table 1). With the exception of the present-day simulation, the insolation states correspond to vertical lines shown in Fig. 1. The summer solstice case shown in Fig. 1 is similar enough to the present-day case that, for an initial study, we decided that an additional simulation was unnecessary.

Table 1. Insolation parameters for the GCM simulations. Titles correspond to: [a]obliquity, [b]eccentricity, [c]L_s of perihelion, [d]mean daily insolation (W/m^2). Colors shown here correspond to simulations in figures throughout the abstract.

GCM Run	ε[a]	e[b]	L_p[c]	Q[d]
Present-day	25.19º	0.0933	251.04º	211.4
Autumn max	23.05º	0.1089	4.601º	235.9
Winter max	24.49º	0.1177	98.38º	215.2
Spring max	23.18º	0.1117	179.13º	237.6

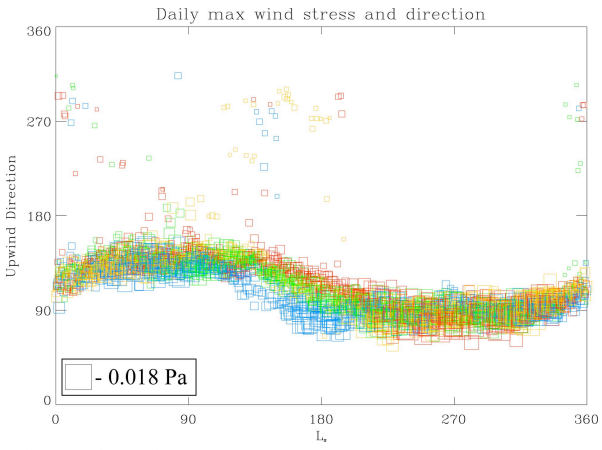

Figure 3. Wind direction and stress in Meridiani Planum. Note that different insolation states produce similar wind patterns.

Results:

GCM simulations: In all the figures that follow, colors correspond to the four GCM simulations listed in Table 1. Figure 3 shows wind direction and stress throughout the martian year at the grid point closest to Opportunity's landing site in Meridiani Planum. All four simulations show approximately the same wind pattern: southeasterly winds dominate from mid-autumn through mid-winter, then shift to easterly winds during spring through mid-summer. There is some suggestion that the summer pattern may begin earlier in the year during the winter solstice simulation ("winter max"), but little else changes.

Figure 4 shows the maximum daily wind stresses throughout the year in Meridiani Planum for each simulation. As with wind direction, there appears to be a season-dependent pattern of wind strength: there is a peak in mid-autumn through early winter and a broader peak in mid-spring through mid-summer. In particular, the "winter max" simulation indicates (compared to the present-day simulation) relatively strengthened autumn/winter winds, and perhaps relatively weaker, but longer-lived winds during spring and summer. The "autumn max" and "spring max" results lie between those of the "winter max" and present-day simulations.

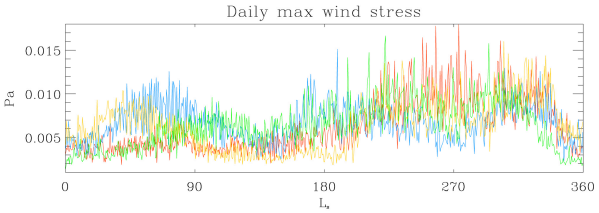

Figure 4. Daily maximum wind stress for each simulation. Note the bimodal distribution of wind stresses and variation among simulations.

Potential sand flux: One way to assess the sand-transporting winds predicted by the GCM is to estimate the potential sand flux through a martian year. Assuming that an infinite source of sand is available for transport, the potential sand flux q may be approximated by the following:

$$q \approx 2.61 \frac{\rho}{g}(u_* - u_{*_t})(u_* + u_{*_t})^2 \quad \text{kg m}^{-1}\,\text{s}^{-1}$$

in which ρ is air density, g is gravitational acceleration, u_* is friction speed, and u_* is the threshold friction speed [22]. Using the classical empirical relation [23], the fluid threshold friction speed in Meridiani Planum is on the order of 1.6 m s^{-1}, a value never exceeded by our GCM simulations. However, recent work suggests that once saltation has been initiated, transport may be maintained at a friction speed (i.e., an "impact friction speed") approximately 10% that of the fluid threshold [24]. Assuming that wind gusts unresolved by the GCM occur and initiate saltation, we use the relation of [24] to estimate the impact threshold friction speed u_{*_t}, and then use this value to calculate potential sand fluxes for each time step in each simulation.

Figure 5 shows the annual potential sand fluxes plotted as rose diagrams. In all four simulations, easterly (summer) winds dominate and southeasterly (winter) winds play a subordinate role of varying significance. The "winter max" and "spring max" simulations can produce noticeably more potential sand flux than the present-day simulation.

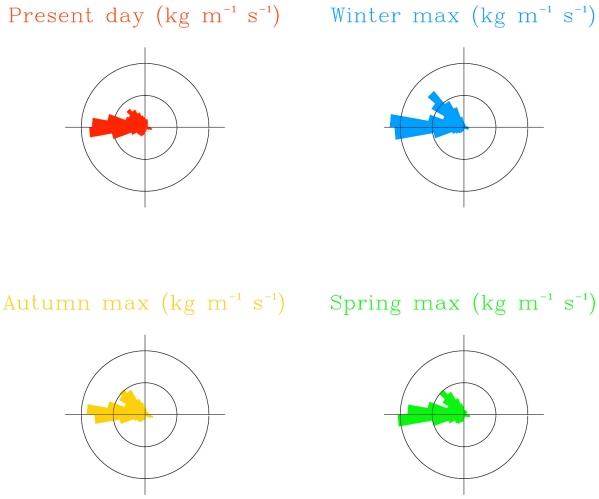

Figure 5. Sand roses indicating annual maximum potential sand transport for each of the four orbital states in Table 1. Easterly winds predominate and southeasterly winds play a minor role that varies in relative strength.

Discussion: Comparing Figures 1 and 5 reveals inconsistencies between GCM predictions and observed wind patterns. Although easterly winds created the coarse-grained ripples, there is no morphological evidence that this wind currently blows at saltation strength; however, the GCM predicts that this wind should dominate sand transport. It is possible that this misalignment of predicted and observed activity is caused by the low resolution of the GCM grid, which often precludes prediction of local-scale winds. In addition, the GCM does not predict northwesterly winds associated with planetary-scale dust events. This is perhaps not surprising, because the GCM simulations did not attempt to simulate atmospheric effects of dust storms. However, this discrepancy highlights the potentially strong influence of atmospheric dust on regional-scale wind patterns, as well as the need for a better understanding of their formation mechanism and development.

Despite the above inconsistencies, there are some intriguing suggestions in the simulated wind patterns.

First, wintertime southeasterly winds match well with the observed activity of the dark wind streaks in Victoria crater. These winds increase in relative strength in the other simulations, suggesting that they may have played a role in changing bedform morphology; for example, these winds may be responsible for the partial realignment of the main coarse-grain ripple crests (cyan arrows in Fig. 1). Second, the relative increase in potential sand flux in the "winter max" and "spring max" simulations may correspond to periods of ancient activation of coarse-grained ripples. If this is the case then we can begin to understand the changes in wind circulation that lead to ripple activations and subsequent stabilization.

Conclusions: To attempt to determine how the local wind patterns in Meridiani Planum vary with insolation state over the past 400 ka, we have run four GCM simulations corresponding to orbital configurations that produce maximum insolation at each of the four main seasons. Results indicate that the wind pattern varies in strength and duration, but not in direction. In all four cases, easterly (southern) summer winds dominate and southeasterly winter winds play a subordinate role.

Although the changes in wind strength are suggestive of possible ancient activation of coarse-grained ripples, present-day wind predictions do not match with observed current saltation activity. Likely reasons for this discrepancy include the low resolution of the GCM (which may be addressed further by mesoscale modeling, see [7]) and a more realistic representation of large dust events.

We intend to continue exploring parameter space by simulating a range of insolation states from the previous 400 ka. Although we will not explicitly simulate a large dust storm, we will change the expected background dust, following the trend of [25]. Finally, mesoscale modeling using these GCM simulations as initial and boundary conditions will help determine smaller-scale flows that the GCM cannot capture.

References: [1] Silvestro, S. et al. (2010) *Geophys. Res. Lett., 37,* L20203, doi:10.1029/2010GL044743. [2] Bridges, N. T. et al. (2012) *Geology, 40*(1), 31-34, doi:10.1130/G32373.1. [3] Geissler, P. E. (2011) *LPS XLII,* Abstract #2537. [4] Fenton, L. K. and Hayward, R. K. (2010) *Geomorphology, 121,* 98-121. [5] Bourke, M. C. and Wray, J. J. (2011) *LPS XLII,* Abstract #2749. [6] Golombek, M. et al. (2010) *J. Geophys. Res., 115,* E00F08, doi:10.1029/2010JE003628. [7] Michaels, T. M. and Fenton, L. K. (2012) *NASA/Ames Wkshp. on Mars Recent Climate Change*, Moffett Field, CA. [8] Sullivan, R. et al. (2007) *LPS XXXVIII,* Abstract #2048. [9] Zimbelman, J. R. et al. (2009) *Icarus, 203,* 71-76. [10] Geissler, P. E. et al. (2010) *JGR, 115,* E00F11, doi:10.1029/2010JE003674. [11] Geissler, P. E. (2008) *JGR, 113,* E12S31, doi:10.1029/2008JE003102. [12] Chojnacki, M. (2011) *JGR, 116,* E00F19, doi:10.1029/2010JE003675. [13] Sullivan, R. et al. (2005) *Nature, 436,* doi:10.1038/nature03641. [14] Jerolmack, D. J. et al. (2006) *JGR, 111,* E12S02, doi:10.1029/2005JE002544. [15] Laskar, J. (2004), *Icarus, 170,* 343-364. [16] Fenton, L. K. and Richardson, M. I. (2001) *JGR, 106,* 32,885-32909. [17] Haberle, R. M. et al. (2003) *Icarus, 161,* 66-89. [18] Haberle, R. M. et al. (2006) *GRL, 33,* L19S04, doi:10.1029/2006GL026188. [19] Haberle, R. M. et al. (1993) *JGR, 98,* 3093-3123. [20] Haberle, R. M. et al. (2011) *4th Int'l. Wkshp. Mars Atmosph.*, 223-226. [21] Hollingsworth, J. L. et al. (2011) *4th Int'l. Wkshp. Mars Atmosph.* 70-73. [22] White, B. R. (1979) *JGR, 84*(B9), 4643-4651. [23] Greely, R. and Iversen, J.D. (1985) *Wind as a Geological Process*, Cambridge Univ. Press. [24] Kok, J. F. (2010) *GRL, 37,* L12202, doi:10.1029/2010GL043646. [25] Haberle, R. M. (2006) *GRL, 33,* L19S04, doi:10.1029/2006GL026188.